

Paper-based spintronics: magneto-resistivity of permalloy onto paper substrates

Meriem Akin, Lutz Rissing
Institute of Micro Production Technology
An der Universitaet 2, 30823 Garbsen, Germany
akin@impt.uni-hannover.de

Abstract

Driven by low-cost, resource abundance and distinct material properties, the use of paper in electronics, optics and fluidics is under investigation. In order to realize a dense coverage of sensor networks as part of the roadmap of the internet-of-things, achieving lower manufacturing cost of the aforementioned sensors is required. Considering micro-electro-mechanical systems based on magneto-resistance principles (anisotropic, giant, tunnel) that are conventionally manufactured onto inorganic semiconductor materials, we propose the use of paper substrates for cost reduction purposes primarily. In particular, we studied the magneto-resistance sensitivity of permalloy (Py:Ni₈₁Fe₁₉) onto paper substrates utilized in various daily applications. Here, the Py:Ni₈₁Fe₁₉ coating was developed by means of, but not limited to, sputter deposition, and spans an area of 10x10 mm² and a thickness of 70 nm. In this research, we investigated several paper materials covering a range of grammage of [80, 350] g/m², surface roughness of [0.21, 3.462] μ m given by the root mean squared R_{rms} , various impregnations, porosity levels and surface macro-structures. Yet, in this paper, we focus on our findings with clean room paper (80 g/m², R_{rms} = 2.877 μ m, 23% surface porosity, latex impregnation, no embossed macro-structure). Employing a four-point-probe resistivity measurement setup, we investigated the change of electrical resistance of Py:Ni₈₁Fe₁₉ under the presence of an oriented external magnetic field. Compared to the theoretical limit of 2.5% of Py:Ni₈₁Fe₁₉ on smooth surfaces, we have obtained large and positive magneto-resistive changes (2.5 - 14%) for these aforementioned systems. Principally, we analyzed the effect of surface topology of the clean room paper on the magneto-resistance sensitivity of Py:Ni₈₁Fe₁₉. We concluded that the occurrence of such magnetic behavior is most probably due to tunneling of electron waves through the asperities and porosity of the paper surface and subsequent scattering of electrons at pinned domain walls.

Introduction

With the digitization of information, paper is moving away from its classical fields of application such as writing and printing of text. Yet, today, paper still exists despite the belief of many visionaries over the centuries [1]. In fact, several disruptive applications of paper have erupted such as the usage of paper tubes in construction of buildings [2], interactive paper newsprints with embedded circuits [3], diagnosis micro-labs made of paper [4], paper-based foldable microscopes [5], etc. [6]. In terms of cost analysis, the average cost of 1 m² of variously engineered paper ranges from [0.10, 2.00] US\$ while the cost of 1 m² of widely used

polyimide films and 1 m² of polished silicon are about 5.00 US\$ and 1,000 US\$ as of 2013 respectively¹. In addition to its low cost, paper is an abundant resource with a wide base of qualifying technical properties (biocompatibility, chemical stability, mechanical bendability etc.). Thus, while paper is being reinvented to a smart physical object with embedded sensors and software, it is compellingly becoming part of the evolving network of the internet-of-things.

In order to achieve high-yield and high-performing systems on paper, various efforts on characterizing paper at macro-, micro- and nanoscales abide ([7], [8], [9]). Besides, new paper types are being fabricated to conform to specialized engineering applications. For instance, a transparent smooth paper (>90% optical transmission and 10 nm surface roughness) was developed and demonstrated in manufacturing opto-electronic devices [10]. By employing vulcanized paper fibers, strong paper was fabricated that was shown to work for mechanically stressed parts in the automotive industry [11]. Also, by multi-layering paper fibers with conductive polymers [12] or growing conductive particles onto paper fibers [13], paper was converted from an insulating carrier to a functional conductor.

In this work, we are interested in employing paper in magnetic based micro-electro-mechanical systems for the aforementioned benefits. In particular, we would like to explore the realization of various magneto-resistance effects such as anisotropic magneto-resistance, giant magneto-resistance, tunnel magneto-resistance etc. onto paper platforms. Hence, we would like to investigate the precision, i.e. uniqueness of magnetic response on paper. We envision paper to make these specialized and mostly expensive spintronic systems such as spin-valve sensors, magnetic compasses and read heads available at a much lower cost for a broader user base. Thus, we study the interplay between the physical properties of paper and the magneto-electric phenomena. Besides, we investigate manufacturability and propose fabrication processes for mass-production purposes.

Prior art on magnetics in paper-based systems

Magnetism as an added value to the existing technical properties of paper has been put for years into practice e.g. in the magnetic bands of subway tickets and parking garage tickets. By chemically synthesizing magnetic ferrites in the suspension of the lumen fibers and stirring rapidly, the internally porous paper fibers are filled with magnetic particles ([14], [15]). In this case, the magnetic functionality is embedded within the body of the fibers, and acts on the

¹ These prices were obtained through quotations of local suppliers in Germany.

entire paper volume. It was reported that these magnetic papers exhibit superparamagnetic behavior [16].

Based on the classical design of spintronics, where magnetic layers are deposited onto inorganic substrates and structured by means of thin film technology to meanders and concentrators, we would like to realize this concept onto paper substrates. In this case, the magnetic functionality is mainly affected by the surface topology of paper unlike the composite paper embedded with magnetic particles, where internal porosity is more crucial. In addition to the internal porosity of paper fibers [17], conventional paper exhibits large surface roughness due to the anisotropic network topology of the fibers (inter-roughness). Besides, each microfibril exhibits nano-roughness and nano-porosity at the surface level (intra-roughness and intra-porosity) (Figure 1).

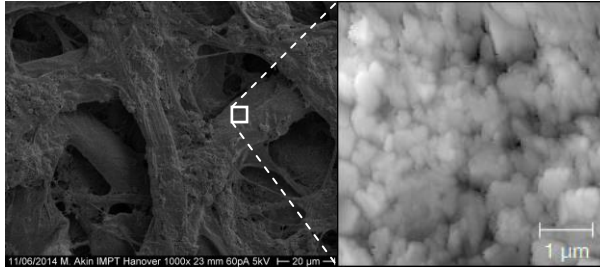


Figure 1 Example of a topology of paper obtained by scanning electron microscopy and atomic force microscopy.

In the following, we review various magnetic phenomena that could occur due to the aforementioned geometrical properties of paper surfaces. In fiber network topologies, domain walls form where fibers/wires meet or change orientation, which can be clearly illustrated on the basis of a semi-circular wire [20]. The presence of domain walls induce scattering of electrons, and therefore electrical resistance [21]. It was also identified that rough surfaces with a network topology allow for domain wall motion easier than rough surfaces without a network topology [18]. In studying artificial spin ice networks, it was observed that each link with a distinct orientation to the magnetic field exhibits locally anisotropic magneto-resistance [23]. Hence, the response of the network is an accumulation of the various local magneto-resistive responses.

Generally speaking, ferromagnetic layers once deposited onto rough surfaces are not expected to exhibit an elemental magneto-resistive response. In this regard, even if not explicitly applied to paper substrates, the impact of surface roughness and surface topology of the substrate on the magnetic behavior of thin layers was thoroughly studied. In the low surface roughness regime (< 10 nm), it was identified that layers deposited on rough surfaces are less sensitive to magnetic fields, which is given by a lower change in magneto-resistance [22]. For intermediate surface roughness regimes (< 100 nm), it was observed that the magnetization reversal depends heavily on the surface roughness, such that the magnetic domain walls once pinned onto rough surfaces can hardly be unpinned, especially with the increase in the ratio of

mean roughness to film thickness ([18], [19]). Hence, the ferromagnetic layer becomes more resistant to the magnetic field, which is usually denoted by a large magnetic coercivity, which is disadvantageous for sensing applications.

Last, we expect the nano-pores of the paper fibrils to form with the surrounding ferromagnetic layer a magnetic tunnel junction or a tunnel magnetoresistance [24]. Similar to the tunneling principle applied in scanning tunnel microscopy [25], tunneling of electrons occurs through the air that is enclosed in the nano-pores.

Experimental

We studied the real-time sensitivity of permalloy (Py: $\text{Ni}_{81}\text{Fe}_{19}$) to magnetic loading when deposited on clean room paper. In order to draw reliable conclusions, we compared the performance of the paper-based system to systems with ascending surface entropies: (1) polished silicon dioxide (SiO_2) substrates, (2) rough SiO_2 substrates and (3) replicas of paper on a stiff epoxy resin.

Materials

We used clean room paper that has a grammage of 80 g/m^2 , a thickness of $79 \text{ }\mu\text{m}$ and a surface roughness given by the root mean squared $R_{\text{rms}} = 2.877 \text{ }\mu\text{m}$ according to the measurement standards DIN EN ISO 4288:1998 (Figure 2). Besides, the paper was impregnated with latex for clean room usage purposes. By computational analysis of the scanning electron microscope image of the paper surface, the surface porosity was determined to be in the range of 23% (Figure 3).

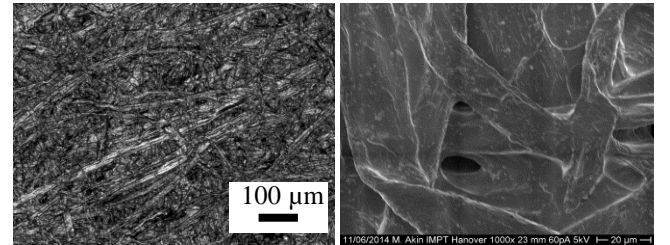


Figure 2 Surface topology of clean room paper obtained by laser microscopy and scanning electron microscopy.

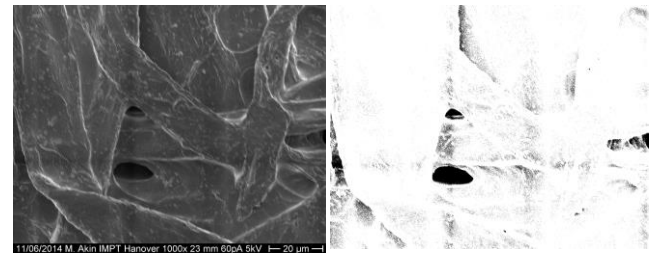


Figure 3 Image recognition of pores from SEM image.

We replicated the surface topology of paper by means of vacuum casting. First, we created a silicone mold of the paper surface. Then, we replicated the surface of the silicone mold onto an epoxy resin (Figure 4 and Figure 5). Due to the effect

of gravity during casting, it should be noted that surface porosity could not be transferred from paper to epoxy. Instead, pores in the paper were transformed to roughness asperities on the epoxy surface. Also, the edges of the epoxy samples were not perfectly straight because they were allowed to remain as free surfaces during the curing process. Besides, the paper master used for replication could not be used for an actual system since it was contaminated and pre-stressed. In terms of mechanical hardness, paper has a hardness of 189.57 MPa, which was obtained by means of nano-indentation experiments (Berkovich tip). In comparison, the epoxy resin has a D1 shore hardness of 85, which translates to app. 688 MPa in nano-hardness [34]. Therefore, we did not expect the very same responses from the paper and the epoxy samples. Yet, the replication was expected to be sufficient to draw some first conclusions regarding surface topology.

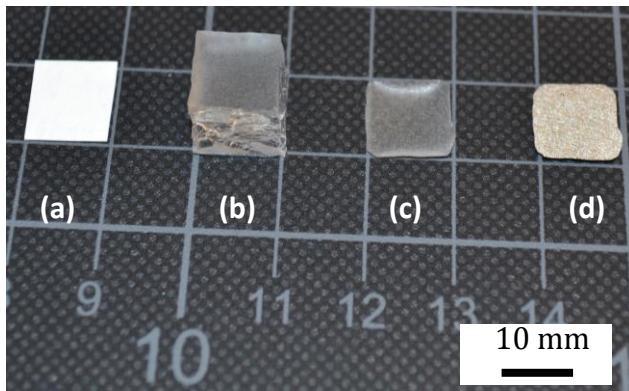


Figure 4 Replication of paper surface topology to an epoxy resin. (a) Original paper material (b) silicone mold after casting (c) epoxy replica of silicone mold (d) epoxy sample coated with Py:Ni₈₁Fe₁₉.

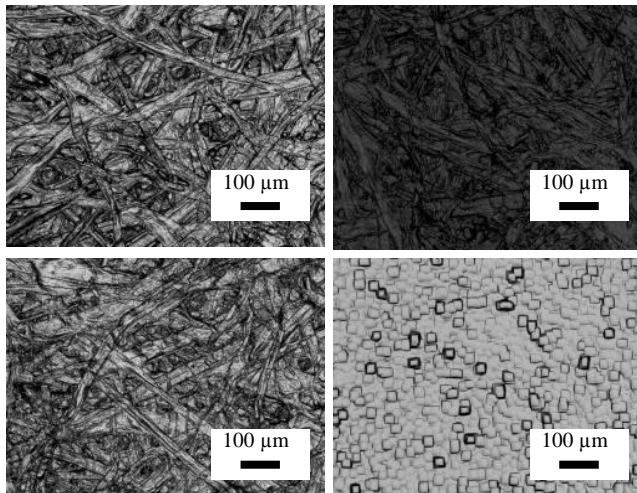


Figure 5 Laser scanning micrographs of the surface topology of paper, $R_{rms} = 2.877 \mu m$ (a), silicone cast (b), epoxy replica, $R_{rms} = 3.235 \mu m$ (c) and rough SiO₂ surface $R_{rms} = 1.430 \mu m$.

(Please note that micrographs (a), (b) and (c) were not taken at consistent locations).

Last, we employed polished and rough SiO₂ as reference surfaces. In particular, 100 nm of SiO₂ was thermally grown onto both sides of a one-side polished p-type <100> silicon wafer of a thickness of 525 μm . Here, boron was used as a dopant.

By means of sputter deposition, we coated the four material platforms with Py:Ni₈₁Fe₁₉. Decisive for the mechanical quality of the coated systems are the differences in coefficients of thermal expansion between the various materials. In this regard, the coefficients of thermal expansion of the paper and Py:Ni₈₁Fe₁₉ were measured using an optical dilatometer (Table 1).

	Silicon	Clean room paper	Py:Ni ₈₁ Fe ₁₉
20°C	2.3	210	-12
50°C	2.7	-921	16
100°C	3	-2816	63
150°C	3.2	-4701	110

Table 1 Coefficients of thermal expansion of paper and Py:Ni₈₁Fe₁₉ obtained from optical dilatometer measurements and those of silicon as reported in [26] (in [ppm/K]).²

Using a vibrating sample magnetometer (VSM), we conducted a comparative study of the dependence of the magnetic properties of Py:Ni₈₁Fe₁₉ on the various substrates that we employed in this work. We prepared 5x10 mm² samples according to the preparation guidelines as described in detail in the next section. We measured three samples of each material combination (Py:Ni₈₁Fe₁₉ on polished SiO₂, Py:Ni₈₁Fe₁₉ on rough SiO₂, Py:Ni₈₁Fe₁₉ on epoxy replication of paper and Py:Ni₈₁Fe₁₉ on paper) at 21°C and 40-70 % relative humidity, and commented on the averaged result.

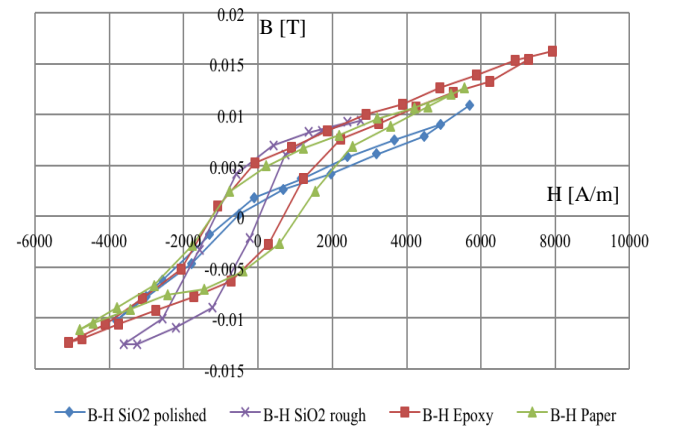


Figure 6 Magnetic hysteresis (magnetic flux density B vs. magnetic field strength H) of Py:Ni₈₁Fe₁₉ as deposited onto polished SiO₂, rough SiO₂, epoxy replica of paper and paper.

As expected, we observed an increase in coercivity³ with the increase in the entropy of the surface topology (Figure 7).

² Remarkable are the negative coefficients of thermal expansion of the clean room paper.

While paper has –in average- a larger coercivity than the epoxy sample, epoxy manifests larger remanence than paper (Figure 8). Most interestingly, paper systems exhibit larger coercivity and larger squareness of magnetic field strength than SiO₂ systems (Figure 9).

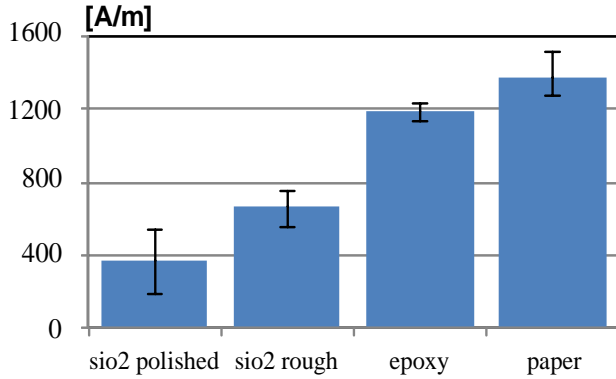


Figure 7 Coercivity of Py:Ni₈₁Fe₁₉ as deposited onto polished SiO₂, rough SiO₂, epoxy replica of paper and paper.

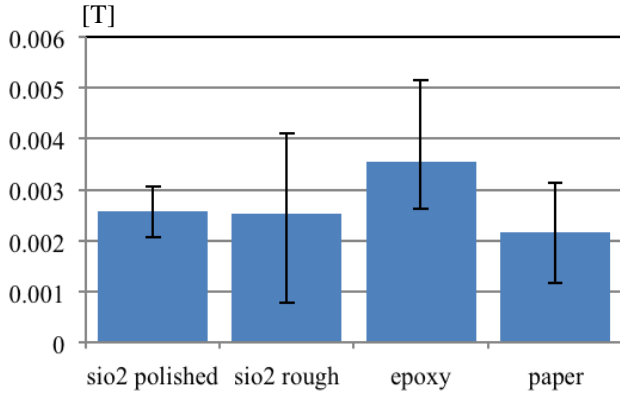


Figure 8 Remanence of Py:Ni₈₁Fe₁₉ as deposited onto polished SiO₂, rough SiO₂, epoxy replica of paper and paper.

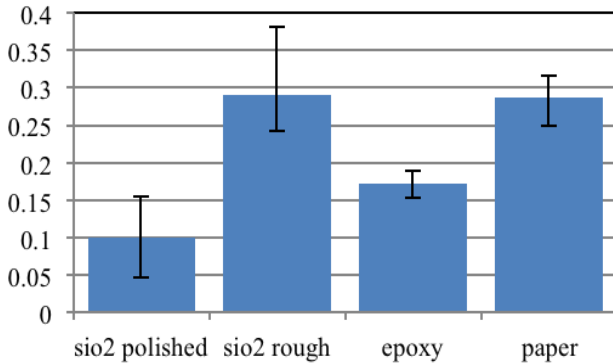


Figure 9 Squareness ratio of magnetic field strength of Py:Ni₈₁Fe₁₉ as deposited onto polished SiO₂, rough SiO₂, epoxy replica of paper and paper.

³ Coercivity, remanence and squareness ratio were averaged over the right and left sections of the hysteresis. The results of the VSM measurements were not corrected using the demagnetization factors.

It should be noted that the theoretical coercivity and remanence values of Py:Ni₈₁Fe₁₉ on SiO₂ were not obtained due to a combination of the following: (1) contamination during the sputter process with other materials, (2) scratches due to handling with tweezers, (3) shape anisotropy of the samples and (4) demagnetizing fields within the Py:Ni₈₁Fe₁₉ coating. Last, we note the consistent asymmetric magnetization reversal (asymmetric hysteresis loops in Figure 8) of all systems, which might be due to the shape asymmetry of the samples [32].

Sample preparation guidelines

In order to exclusively study the effect of surface topology onto the magneto-resistance of the clean room paper, we omitted or alleviated as much as possible the occurrence of interfering phenomena due to sample preparation. First, we prepared square-shaped samples of the size of 10x10 mm², decreasing the effect of surface anisotropy onto the magneto-resistance measurements. Clearly, it would have been preferable to work with circular samples.

It was observed that machining of substrates after deposition of magnetic layers created boundary defects and geometrical singularities in the magnetic layer, which affect the magnetic performance of the system [27]. Since we employed materials that were machined with different techniques (dicing for SiO₂ and cutting for paper), we machined the substrates prior to sputter deposition. The epoxy samples were fabricated in required size and did not go through any additional machining after coating.

Next, we minimized the occurrence of large mechanical stresses within the Py:Ni₈₁Fe₁₉ coating due to mismatches in thermal expansion when cooling down after the sputter deposition process (Table 1). Besides, the paper, epoxy and rough SiO₂ substrates were expected to release layer stress easier –in this order- than polished SiO₂ due to mechanical interlocking between Py:Ni₈₁Fe₁₉ and the substrates. In order to eliminate preferential stress formation, we employed a low-power sputtering process (50 W) such that the substrate and layer temperature remained below 50°C.

All samples (four of each material configuration) were prepared within one single sputter deposition process. In this case, we removed any fluctuations in layer thickness and chamber conditions from batch to batch. In order to preserve the material surface topology, we deposited Py:Ni₈₁Fe₁₉ layers of a thickness of 70 nm (<R_{rms} of the rough substrates). Last, in order to avoid the effect of preceding magnetization of Py:Ni₈₁Fe₁₉ prior to measurement, we measured each sample only once under the application of an external magnetic field.

Measurement set-up

We used a four-point-measurement setup built within a concentrated magnetic field of the size of 18.8 x 20.45 x 29.44 mm³ (Figure 10). By inducing an electric current into wire wound coils around a hard magnetic metal, the magnetic field was created (Figure 10). A maximum magnetic intensity of 90 kA/m (~1100 Oe) could be applied with this setup. Yet, due to inhomogeneity of the magnetic field due to limited size

of the field region (Figure 11), a maximum of 60 kA/m (~800 Oe) was applied at the four-point-probe location. Each measurement cycle started at -60 kA/m. At discrete steps of 2 kA/m, the magnetic intensity was swept to 60 kA/m and back to -60 kA/m. Each discrete magnetic intensity was held constant for 1 ms before sweeping continues to allow for transient transition between two discrete magnetic intensities.

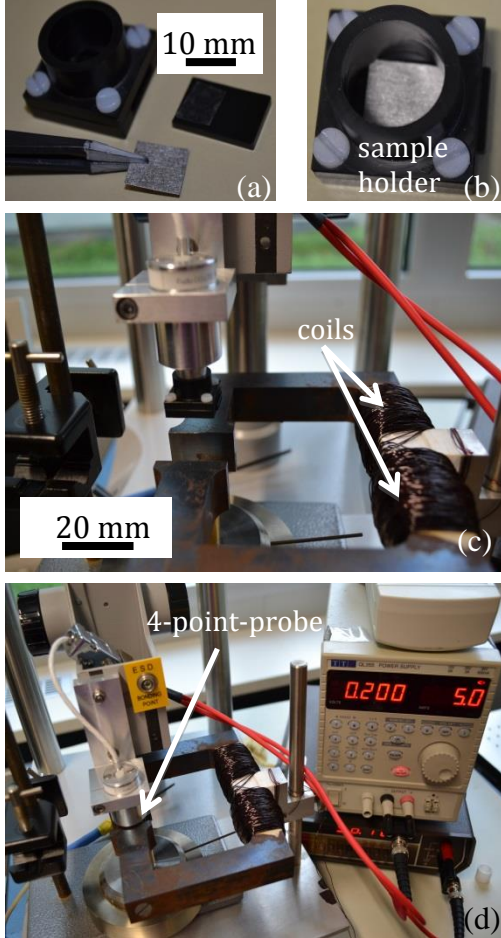


Figure 10 (a) Handling of sample, (b) sample holder to prohibit paper from bending, (c) descending of four-point-probe into magnetic field, (d) induction of constant electric current into coils and creation of magnetic field.

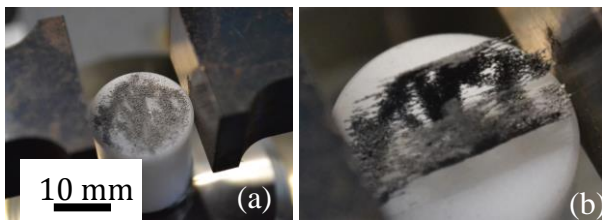


Figure 11 (a) Iron particles before application of magnetic field, (b) visualization of magnetic field with iron particles at maximum magnetic intensity of the measurement setup at the 4-point-probe measurement location.

Since $\text{Py:Ni}_{81}\text{Fe}_{19}$ conventionally manifests anisotropic magneto-resistance, we measured the resistance of $\text{Py:Ni}_{81}\text{Fe}_{19}$ in two electric current-to-magnetic-field configurations. First, we measured the parallel configuration: The flow orientation of the electric current applied to $\text{Py:Ni}_{81}\text{Fe}_{19}$ is parallel to the lines of the magnetic field. Then, we measured the perpendicular configuration: The flow orientation of the current applied to $\text{Py:Ni}_{81}\text{Fe}_{19}$ is perpendicular to the lines of the magnetic field.

During the measurements, the ambient temperature and relative humidity were regulated at 21°C and 40-70 % respectively. Besides, we handled all samples using tweezers in order to not induce any thermal perturbation to the system.

We measured the absolute and relative magneto-resistance coefficients as given by:

$$\text{MR}_a = 100 \cdot (R_{\max} - R_{\min})/R_{\max}, \text{ and} \quad (1)$$

$$\text{MR}_r = 100 \cdot (R_c - R_{\min})/R_{\min}, \quad (2)$$

respectively. R_{\max} and R_{\min} are the maximum and minimum electrical resistances recorded through the measurement cycle. R_c is the instantaneous electrical resistance.

Noise analysis and measurement errors

While considering our measurement results, we would like to point out sources of error during measurement that we were not able to control despite extreme caution. First, the co-centric positioning of the sample to the 4-point-probe was done manually. Hence, the position of the four-point-probe slightly deviated from the center of the sample with small, yet different, amounts at each experiment. Besides, a remaining magnetization of 1.7 kA/m was present in the magnetic region even when the measurement setup was not in operation. The latter was due to the hard magnetic material used to redirect and focus the magnetic field. Thus, samples when positioned into the measurement setup were first subject to the remaining magnetic field.

The four-point-probe disposes of rounded needles with a radius of 500 μm that are individually biased by a spring load of 1-2 N/mm^2 . After measurement, we observed a remaining indented area in the soft systems like paper and epoxy (Figure 13). A cracking of $\text{Py:Ni}_{81}\text{Fe}_{19}$ due to indentation and an increase in the primary electrical resistance of $\text{Py:Ni}_{81}\text{Fe}_{19}$ around the gauss probes were therefore expected. Besides, we observed slight scratching of $\text{Py:Ni}_{81}\text{Fe}_{19}$ onto the SiO_2 substrates (Figure 12), which induced shunt resistances as well.

In order to estimate the order of magnitude of the regular shunt resistances occurring in the SiO_2 -based system, we measured the electrical resistance of the bare SiO_2 substrates. Let $R_{\text{Py:Ni}_{81}\text{Fe}_{19}}$, R_{SiO_2} and R_{total} be the electrical resistances of the $\text{Py:Ni}_{81}\text{Fe}_{19}$ coating, the SiO_2 substrate and the total of the parallel resistances $\text{Py:Ni}_{81}\text{Fe}_{19}$ and SiO_2 ($(R_{\text{SiO}_2} + R_{\text{Py:Ni}_{81}\text{Fe}_{19}})/(R_{\text{SiO}_2} \cdot R_{\text{Py:Ni}_{81}\text{Fe}_{19}})$). In the case of polished SiO_2 substrates, we determined a ratio of $(R_{\text{total}} / R_{\text{SiO}_2}) = 0.44$. For rough SiO_2 substrates, we obtained a ratio of $(R_{\text{total}} / R_{\text{SiO}_2}) =$

0.02. Consequently, we deduce that the polished SiO₂ systems are more susceptible to shunt resistances.

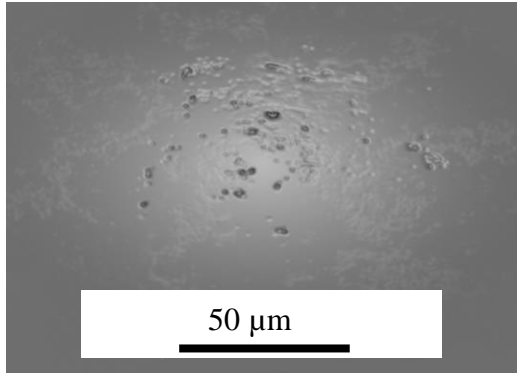


Figure 12 Scratches in Py:Ni₈₁Fe₁₉ on SiO₂ substrate at a needle location.
(The image was processed using artistic filters to display the defects more clearly)

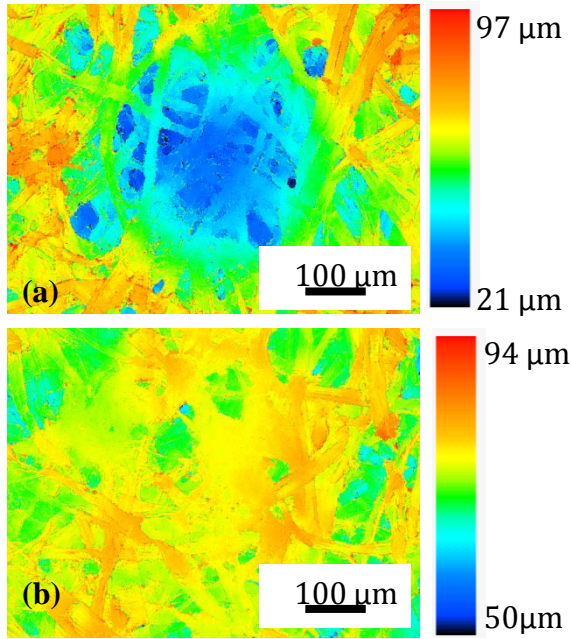


Figure 13 Remaining indentation on paper surface (a) and epoxy surface (b) after four-point-measurement.

In addition, we expected the occurrence of additional noise in the measurements. Since we did not explore the demagnetization of the samples in this work, repetitive measurements of the same sample for canceling out noise were not possible. In this regard, we explored solely the noise originating from the set-up in the absence of all inputs (sample, electrical current and operated magnetic field). By applying the four-point probe to the insulating bottom support to the samples, used during actual measurement, we track the fluctuations V_i in n voltage measurements by the four-point-probe, where $n = 70$. In both measurement configurations, we recorded average deviations of $((\sum V_i^2)/n)^{1/2} = 0.64$ mV, which translate to a 6.24 %-deviation for polished SiO₂-based

systems, 5.17 %-deviation for rough SiO₂-based systems, up to a 2.2 %-deviation for the epoxy-based systems and a maximum deviation of 1.12 % for the paper-based systems.

Results and discussion

Classical anisotropic magneto-resistance of 70 nm of Py:Ni₈₁Fe₁₉ on paper was not observed. Changes in the magneto-resistance were positive and of the order of 2.5-14% (Figure 14 and Figure 15). The expected tunneling of electron waves through the intra-porosity and -roughness of the paper and scattering at the domain walls explain the magneto-resistive behavior of the paper-systems. Yet, two different paper systems did not exhibit identical orders of magnitude of magneto-resistance due to the stochastic variation of the surface topology.

When comparing the magneto-resistive behavior of paper to the epoxy replica, we observed similar phenomenological behavior, most probably due to the macroscopic similarity of the surface topology. In particular, the shape of the evolution of the magneto-resistance possessed similar features such as the remaining change –magnetic memory- in magneto-resistance after the end of the measurement cycle. Yet, the paper exhibited in average a higher change in magneto-resistance than the epoxy replica (Figure 16 and Figure 17). We believe that the large difference in magneto-resistance between paper and epoxy replica was due to the missing porosity on the epoxy surface, and therefore less electron tunneling and scattering.

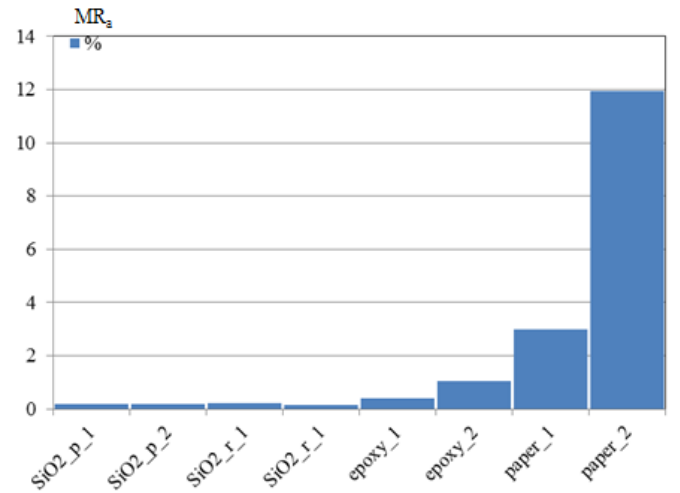


Figure 14 Absolute magneto-resistance coefficient MR_a measured in the parallel configuration for two samples of each polished SiO₂ (sio2_p_1 and sio2_p_2), non-polished SiO₂ (sio2_r_1 and sio2_r_2), epoxy replication of paper (epoxy_1 and epoxy_2) and paper (paper_1 and paper_2).

The noise analysis and the measurement results confirmed that the measurement set-up was not suitable for the SiO₂ systems. As shown in Figure 14 and Figure 15, the polished SiO₂ systems did neither exhibit the practical 1-2% of absolute magneto-resistance [33] nor anisotropic magneto-resistance [28]. In addition to regular shunt resistances [30]

and the large relative measurement noise, we expect the formation of Schottky shunts at the edges of the samples for both polished and rough SiO_2 surfaces. Due to irregular chipping when dicing [29], the SiO_2 layer fractured revealing the underlying p-doped silicon. Since we conducted coating after dicing, $\text{Py:Ni}_{81}\text{Fe}_{19}$ was deposited in intimate contact with the silicon at the edges of the samples. Therefore, Schottky diodes most probably formed at the edges [31], and falsified the magneto-resistance results of $\text{Py:Ni}_{81}\text{Fe}_{19}$.⁴

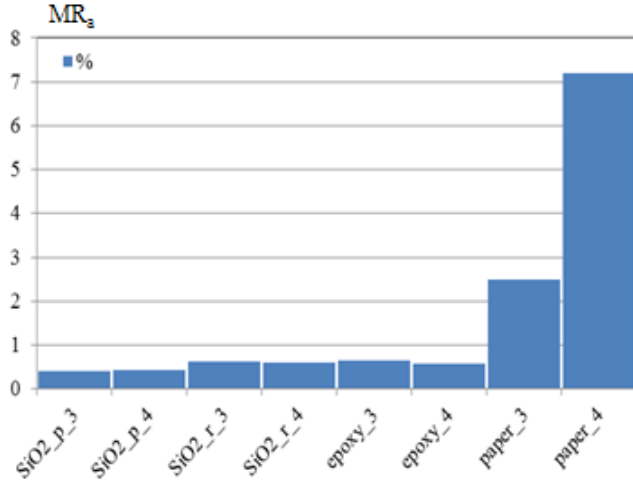


Figure 15 Absolute magneto-resistance coefficient MR_a measured in perpendicular configuration for two samples of each polished SiO_2 (sio2_p_3 and sio2_p_4), non-polished SiO_2 (sio2_r_3 and sio2_r_4), epoxy replication of paper (epoxy_3 and epoxy_4) and paper (paper_3 and paper_4).

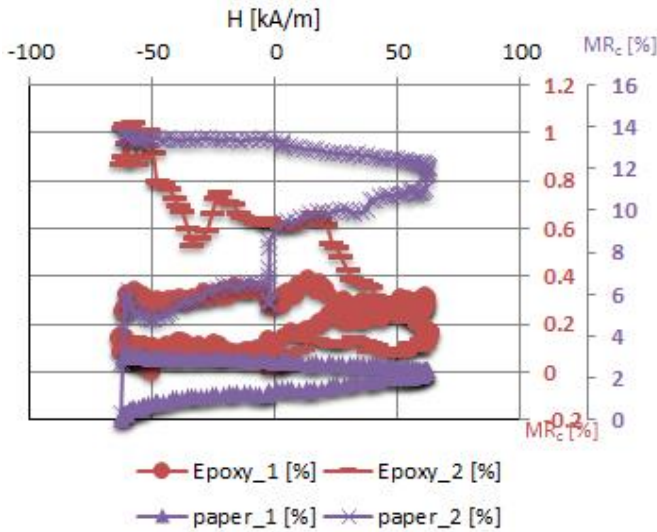


Figure 16 Evolution of coefficient of magneto-resistance MR_r in parallel configuration for two samples of each epoxy replication of paper (epoxy_1 and epoxy_2) and paper (paper_1 and paper_2).

⁴ Since the measurements of $\text{Py:Ni}_{81}\text{Fe}_{19}$ on SiO_2 were perverted due to the exposure of $\text{Py:Ni}_{81}\text{Fe}_{19}$ to silicon, future work will employ reference samples of $\text{Py:Ni}_{81}\text{Fe}_{19}$ deposited on pure fused silica.

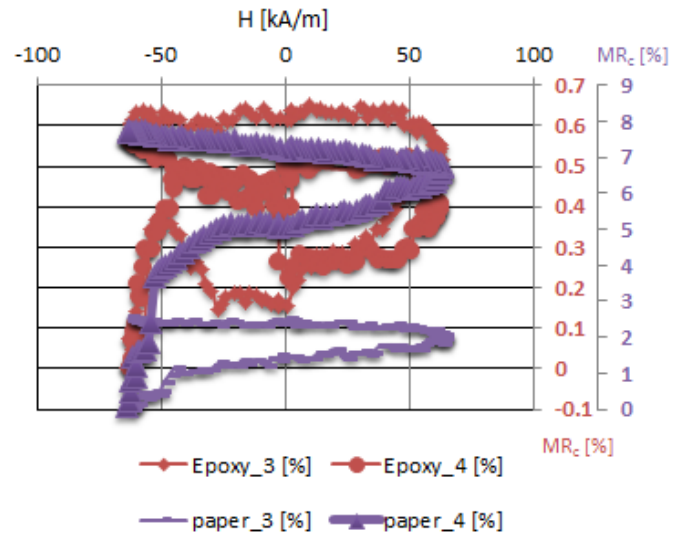


Figure 17 Evolution of coefficient of magneto-resistance MR_r in perpendicular configuration for two samples of each epoxy replication of paper (epoxy_3 and epoxy_4) and paper (paper_3 and paper_4).

Conclusions

In this work, we assessed the magnetic behavior of $\text{Py:Ni}_{81}\text{Fe}_{19}$ onto paper substrates. Compared to the theoretical limit of 2.5% of $\text{Py:Ni}_{81}\text{Fe}_{19}$ on smooth surfaces, we have obtained large and positive magneto-resistive changes (2.5 -14%) for these aforementioned systems. Preliminary explanations for the occurrence of such behavior are tunneling of electron waves through the asperities and porosity of the paper surface and subsequent scattering of electrons at pinned domain walls. We argue that these paper-based systems will find interesting applications, especially due to the rapid magnetic switching we have observed in this work. Based on these promising results, we plan to further investigate the physics behind the large changes in magneto-resistance of $\text{Py:Ni}_{81}\text{Fe}_{19}$ onto paper substrates. Besides, we plan to develop de-magnetization techniques and thorough noise analysis to assess the precision and uniqueness of the response of these paper-based systems.

Acknowledgments

This work was supported by the German Research Foundation within the scope of the collaborative research center CRC/TR123 Planar Optoelectronic Systems. We would like to thank Elke Pichler from the Energy Research Center of Lower Saxony at Technical University of Clausthal for conducting the optical dilatometer measurements. Also, we would like to thank Tanja Marjov from the Institute of Micro Production Technology for conducting the nano-indentation experiment. Last, we would like to thank Piriya Taptimthong, Rahel Kruppe, Anja Wienecke and Lisa Jogschies from the Institute of Micro Production Technology and Sami Akin from the Institute of Communications Technology at Leibniz Universität Hannover for helpful discussions.

References

1. G. Zorpette, "The pitfalls of prediction," *IEEE Spectrum*, pp. 5-6, Jun. 2013.
2. S. Ban and K. Shodhan, "Paper-Tube Housing," *Perspecta*, vol. 34, pp. 154-155+158-159, 2003.
3. K. Stone, "Touch-sensitive input device," *United states Patent Application*, 14/382520, Jan. 2015.
4. A. W. Martinez, S. T. Phillips, M. J. Butte and G. M. Whitesides, "Patterned paper as a platform for inexpensive, low-volume, portable bioassays," *Angewandte Chemie*, vol. 46, no. 8, pp. 1318-1320, Feb. 2007.
5. J. S. Cybulski, J. Clements and M. Prakash, "Foldscope: Origami-based paper microscope," *PLOS one*, vol. 9, no. 6, pp. 1-11, Jun. 2014.
6. D. Tobjörk and R. Österbacka, "Paper electronics," *Advanced Materials*, vol. 23, no. 17, pp. 1935-1961, May 2011.
7. J. Chen, J. Neumann and E. Dörsam, "Investigation on deformation of paper in Z-direction," *Progress in paper physics seminar*, pp. 79-83, Sep. 2014.
8. W. J. Fischer, C. Lorbach, M. Jajcinovic, U. Hirn and W. Bauer, "Measured and calculated bending stiffness of individual fibers," *Progress in paper physics seminar*, pp. 18-23, Sep. 2014.
9. M. Alimadadi and T. Uesaka, "Exploring one more dimension of paper: properties of 3D-oriented fiber network," *Progress in paper physics seminar*, pp. 18-23, Sep. 2014.
10. H. Zhu, Z. Fang, C. Preston, Y. Li and L. Hu, "Transparent paper: fabrications, properties, and device applications," *Energy and Environmental Science*, vol. 7, pp. 269-287, Nov. 2013.
11. B. Künne, U. Willms, C. Stumpf, "Vulcanized fiber as a high-strength construction material for highly loaded construction units," *Progress in paper physics seminar*, pp. 319-321, Sep. 2011.
12. H. J. Youn, J. Lee, J. Ryu, K. Sim and H. L. Lee, "Improvement of conductivity of paper through Layer-by-layer multilayering of PEI and PEDOT:PSS," *Progress in paper physics seminar*, pp. 327-329, Sep. 2011.
13. S. Ge, W. Liu, L. Ge, M. Yan, J. Yan, J. Huang and J. Yu, "In situ assembly of porous Au-paper electrode and functionalization of magnetic silica nanoparticles with HRP via click chemistry for Microcystin-LR immunoassay," *Biosensors and Bioelectronics*, vol. 49, pp. 111-117, Nov. 2013.
14. J. A. Carrazana-Garcia, M. Arturo Lopez-Quintela and J. Rivas Rey, "Ferrimagnetic paper obtained by in situ synthesis of substituted ferrites," *IEEE Transactions on Magnetics*, vol. 31, no. 6, pp. 3126-3130, Nov. 1995.
15. C.H. Chia, S. Zakaria, S. Ahmad, M. Abdullah and S. Mohd Jani, "Preparation of magnetic paper from kenaf: Lumen loading and in situ synthesis method," *American Journal of Applied Sciences*, vol. 3, no. 3, pp. 1750-1754, 2006.
16. W.-B. Wu, Y. Jing, M.-R. Gong, X.-F. Zhou and H.-Q. Dai, "Preparation and properties of magnetic cellulose fiber composites," *Bioresources*, vol. 6, no. 3, pp. 3396-3409, 2011.
17. B. Anderasson, J. Forström and L. Wagberg, "The porous structure of pulp fibres with different yields and its influence on paper strength," *Cellulose*, vol. 10, pp. 111-123, 2003.
18. M. Li, Z.-P. Yhao and G.-C. Wang, "Effect of surface roughness on magnetization reversal of Co films on plasma-etched Si(100) substrates," *Journal of Applied Physics*, vol. 83, no. 11, pp. 6287-6289, Jun. 1998.
19. V. I. Malyutin, V. E. Osukhovskii, y. D. Vorobiev, a. G. Shishkov and V. V. Yudin, "Structure and magnetic properties of etched NiFeCo films," *Physica Status Solidi (a)*, vol. 65, no. 1, pp. 45-42, May 1981.
20. C. Chapper and T. Devolder, "Condensed-matter physics: a magnetic pendulum," *Nature*, vol. 432, pp. 162, Nov. 2004.
21. P. M. Levy and S. Zhang, "Resistivity due to domain wall scattering," *Physical Review Letters*, vol. 79, no. 25, pp. 5110-5113, Dec. 1997.
22. G. Choe and M. Steinback, "Surface roughness effects on magnetoresistive and magnetic properties of NiFe thin films," *Journal of Applied Physics*, vol. 85, no. 8, pp. 5777-5779, Apr. 1999.
23. B. L. Le, D. W. Rench, R. Misra, L. O'Brien, C. Leighton, N. Samarth and P. Schiffer, "Effects of exchange bias on magnetotransport in permalloy kagome artificial spin ice," *New Journal of Physics*, vol. 17, pp. 1-7, 2015.
24. M. Julliere, "Tunneling between ferromagnetic films," *Physics Letters A*, vol. 54, no. 3, pp. 225-226, Sep. 1975.
25. J. Ahn and M. Pyo, "Comparison of STM barrier heights on HOPG in Air and Water," *Bulletin of the Korean Chemical Society*, vol. 21, n. 6, pp. 644-646, 2000.
26. Y. Okada and Y. Tokumaru, "Precise determination of lattice parameter and thermal expansion coefficient of silicon between 300 and 1500 K," *Journal of Applied Physics*, vol. 56, no. 2, pp. 314-320, Jul. 1984.
27. I. T. Collier, M. R. J. Gibbs and N. Seddon, "Laser ablation and mechanical scribing in the amorphous alloys VAC 6030 and METGLAS 2605 SC," *Journal of Magnetism and Magnetic Materials*, vol. 111, no. 3, pp. 260-272, Jun. 1992.
28. W. Thomson, "On the electro-dynamic qualities of metals: -Effects of magnetization on the electrical conductivity of nickel and iron," *Proceedings of the Royal Society of London*, vol. 8, pp. 546-550, Jun. 1857.
29. S. Y. Luo and Z. W. Wang, "Studies of chipping mechanisms for dicing silicon wafers," *International Journal of Advanced Manufacturing Technology*, vol. 35, pp. 1206-1218, 2008.
30. S. A. Correia, J. Lossen and M. Bähr, "Eliminating shunts from industrial silicon solar cells by spatially resolved analysis." *Proceedings of the 21st European Photovoltaic Solar Energy Conference*, 2006.
31. O. Breitenstein, J. P. Rakotoniaina, M. H. Al Rifai and M. Werner, "Shunt types in crystalline silicon solar cells,"

Progress in Photovoltaics: Research and Applications,
vol. 12, pp. 529-538, Jul. 2004

32. Z. Yan, X. Fan and Z. Li, "Magnetization reversal in asymmetric trilayer dots: effect of the interlayer magnetostatic coupling", *Nanoscale research letters*, vol. 9, no. 1, pp. 106, Mar. 2014
33. W. Kwiatkowschi and S. Tumansk, "The permalloy magnetoresistance sensors –properties and applications", *Journal of Physics E: Scientific Instruments*, vol. 19, no. 7, pp. 502-515, 1986
34. subtech.com, "Hardness conversion table", [www](http://www.subtech.com).